MAGNETIC FIELD CONFINEMENT IN THE SOLAR CORONA. I. FORCE-FREE MAGNETIC FIELDS

N. Flyer,[1] B. Fornberg,[2] S. Thomas,[1] and B. C. Low[3]

ABSTRACT

Axisymmetric force-free magnetic fields external to a unit sphere are studied as solutions to boundary value problems in an unbounded domain posed by the equilibrium equations. It is well known from virial considerations that stringent global constraints apply for a force-free field to be confined in equilibrium against expansion into the unbounded space. This property as a basic mechanism for solar coronal mass ejections is explored by examining several sequences of axisymmetric force-free fields of an increasing total azimuthal flux with a power-law distribution over the poloidal field. Particular attention is paid to the formation of an azimuthal rope of twisted magnetic field embedded within the global field, and to the energy storage properties associated with such a structure. These sequences of solutions demonstrate (1) the formation of self-similar regions in the far global field where details of the inner boundary conditions are mathematically irrelevant, and (2) the possibility that there is a maximum to the amount of azimuthal magnetic flux confined by a poloidal field of a fixed flux anchored rigidly to the inner boundary. The nonlinear elliptic boundary value problems we treat are mathematically interesting and challenging, requiring a specially designed solver, which is described in the Appendix.

Subject headings: MHD — Sun: corona — Sun: coronal mass ejections (CMEs) — Sun: magnetic fields

1. INTRODUCTION

A magnetic field has a basic tendency to expand and fill a maximal volume in an electrically highly conducting plasma (Parker 1979; Low 2001). This tendency is driven by magnetic and plasma pressures until force equilibrium is attained both inside the volume and at its boundary with its surroundings. The rigid container wall of a laboratory plasma system provides a reaction force for its confinement. In an open astrophysical atmosphere, there are no external rigid walls, of course. In its far regions, inward forces are usually negligible, and the existence of an equilibrium for a magnetic structure in such an atmosphere depends on an anchoring effect of the stellar surface and the structure's internal force balance. The open atmosphere is physically distinct from rigid-wall confinement in that certain constraints apply for a magnetic structure to be self-confining. Failing confinement, a part of the structure will be ejected out of the atmosphere in order that the residual part can meet these constraints and relax into an equilibrium state. This has been suggested to be at the root of coronal mass ejections (CMEs), a hydromagnetic phenomenon occurring 1 to 3 times a day in the solar corona (Howard et al. 1985, 1997; Hundhausen 1999; Low 1996, 2001).

Consider a theoretical static atmosphere in the one-fluid hydromagnetic approximation described by the force-balance equation

$$\frac{1}{4\pi}(\nabla \times \boldsymbol{B}) \times \boldsymbol{B} - \nabla p - \frac{\rho GM_\odot}{r^2}\hat{\boldsymbol{r}} = 0, \tag{1}$$

$$\nabla \cdot \boldsymbol{B} = 0, \tag{2}$$

[1] National Center for Atmospheric Research, Division of Scientific Computing, 1850 Table Mesa Drive, Boulder, CO 80305; flyer@ucar.edu, thomas@ucar.edu.
[2] Department of Applied Mathematics, 526 UCB, University of Colorado, Boulder, CO 80309; fornberg@colorado.edu.
[3] National Center for Atmospheric Research, High Altitude Observatory, 345 Mitchell Lane, Boulder, CO 80307; low@ucar.edu.

where p, ρ, and $\boldsymbol{B}$ are, respectively, the plasma pressure, plasma density and magnetic field. We present a hydromagnetic study of the self-confinement of magnetic fields in the unbounded region outside a sphere of radius r_0 in the force-free approximation

$$(\nabla \times \boldsymbol{B}) \times \boldsymbol{B} = 0, \tag{3}$$

taking the atmosphere to be so tenuous that we may neglect the pressure and gravitational forces (Lüst & Schüler 1954). These forces may be viewed as higher order effects associated with a small departure from the exact force-free state. We rewrite equation (3) in the form

$$-\nabla\left(\frac{1}{2}B^2\right) + (\boldsymbol{B}\cdot\nabla)\boldsymbol{B} = 0, \tag{4}$$

showing a balance between the forces due to the magnetic pressure and magnetic tension. A reaction force at the inner boundary $r = r_0$ is involved in the global equilibrium. As we show below, equilibrium can exist only if there is a significant amount of magnetic flux anchored to the unit sphere. The outward magnetic pressure force is globally countered by the tension force arising from the strapping effect of that anchored flux.

In a paper to follow (N. Flyer et al. 2004, in preparation), we will account for plasma pressure and gravitational forces and show how they modify in physically interesting ways the results we present here. The goal of both studies is the mathematical demonstration of equilibrium states, by explicit solutions, with an interest in the formation of a rope of twisted magnetic flux levitating in the open atmosphere. The equilibrium of such a structure presents formidable nonlinear boundary value problems, even under the simplifying assumption of axisymmetry. The intuition developed out of examining explicit solutions is one way to gain some insight into how equilibrium confinement may fail, to result in the expulsion of such a flux rope to produce a solar CME (Gibson & Low 1998, 2000; Dere et al. 1999; Ciaravella et al. 2000; Low 2001; Wolfson & Saran 1998; Zhang & Low 2004).

In § 2, we formulate the boundary value problem for an axisymmetric force-free magnetic field, laying down the physical basis for the model. In § 3, we introduce the numerical solver, described in the Appendix, to be used in the construction of the explicit solutions. Families of explicit solutions are presented in § 3 and analyzed in the physical context of a solar magnetic flux rope. In § 4, the results are summarized to arrive at several physical conclusions.

2. FORCE-FREE MAGNETIC FIELDS

Consider the axisymmetric magnetic field written in spherical coordinates and satisfying equation (2)

$$\boldsymbol{B} = \frac{1}{r\sin\theta}\left[\frac{1}{r}\frac{\partial A}{\partial\theta}\hat{\boldsymbol{r}} - \frac{\partial A}{\partial r}\hat{\boldsymbol{\theta}} + Q\hat{\boldsymbol{\varphi}}\right], \quad (5)$$

in terms of a flux function A and a scalar function Q to describe the azimuthal field component. The force-free equation (3) then describes equilibrium in the r-θ plane in terms of a balance between a force due to the poloidal field as represented by the flux function A and the force of the isotropic pressure $\frac{1}{2}Q^2$ contributed by the toroidal component B_φ

$$\left[\frac{\partial^2 A}{\partial r^2} + \frac{\sin\theta}{r^2}\frac{\partial}{\partial\theta}\left(\frac{1}{\sin\theta}\frac{\partial A}{\partial\theta}\right)\right]\nabla A + Q\nabla Q = 0. \quad (6)$$

Setting the Lorentz force in the φ-direction to be zero imposes the condition $Q(r,\ \theta) = Q(A)$, whereupon we obtain the elliptic partial differential equation for A

$$\frac{\partial^2 A}{\partial r^2} + \frac{\sin\theta}{r^2}\frac{\partial}{\partial\theta}\left(\frac{1}{\sin\theta}\frac{\partial A}{\partial\theta}\right) + Q\frac{dQ}{dA} = 0. \quad (7)$$

With each prescription of the functional form of $Q(A)$, equation (7) is to be solved for A subject to suitable boundary conditions.

For the unbounded domain $r > r_0$, we impose the Dirichlet boundary conditions

$$A(r = r_0,\ \theta) = B_0 r_0^2 F(\theta),$$
$$|\nabla A(r,\ \theta)| \to 0 \quad \text{as} \quad r \to \infty,$$
$$A(r,\ \theta = 0 \quad \text{and} \quad \pi) = 0, \quad (8)$$

where F is given. In this paper we treat the case of

$$F = \sin^2\theta, \quad (9)$$

which we refer to as the dipolar case.

The physical interpretation of solutions to the force-free equation (7) requires caution, as emphasized by Wolfson (2003). A distinction needs to be made between a continuous sequence of solutions generated by varying a free parameter in $Q(A)$, taken with a fixed functional dependence on A, and a physical sequence of solutions representing a quasi-static evolution of a field through a continuum of equilibrium states. The former has been called the generating function approach. The latter has been considered in the context of a field evolving in response to boundary motion under conditions of perfect electrical conductivity. Under these conditions, the topology of the evolving field can have no change other than that introduced through the shearing boundary motions acting on field lines threading the boundary. In general, any prescribed form of $Q(A)$ with varying free parameters may not

generate solution sequences that meet such a requirement, and, in such cases, the sequence do not describe a physically acceptable evolution. This point was made by Klimchuk & Sturrock (1989) in criticism of a model of evolving force-free magnetic fields published by Low (1977); see also the reply to this criticism in Low (1990).

Instead of the generating function approach, a physical evolution may be constructed by specifying the field topology of the evolving field, rather than specifying the scalar function $Q(A)$. This can be accomplished either by a reformulation of the force-free equation in the form of a integral-partial differential equation in which $Q(A)$ is left as an unknown (e.g., Low 1978) or by the use of Clebsch variables (Antiochos, DeVore, & Klimchuk 1999). Both of these reformulations lead to mathematically formidable problems.

The scope of our paper is limited to full surveys of solutions to equation (7) for fixed functional forms of $Q(A)$, without taking a sequence of solutions generated in this manner to necessarily imply a physical evolution. Our primary motive is to understand such force-free states through explicit solutions, a reasonable first step in view of the paucity of known solutions to equation (7). As we show, our solutions do provide some useful insights into the nature of force-free fields in the unbounded domain and their capacity to store magnetic energy.

2.1. Potential and Linear Force-free Magnetic Fields

If we set $Q = 0$ for a poloidal field in the dipolar case, the solution to equation (7)

$$A_{\text{pot}} = B_0 r_0^3 \frac{\sin^2\theta}{r}, \quad (10)$$

satisfying the prescribed boundary conditions, describes a potential dipole field in $r > r_0$. This is the lowest energy state of all possible magnetic fields, satisfying those boundary conditions.

If we set $Q = \lambda_0 A$ for some constant λ_0, equation (7) takes the linear form

$$\frac{\partial^2 A}{\partial r^2} + \frac{\sin\theta}{r^2}\frac{\partial}{\partial\theta}\left(\frac{1}{\sin\theta}\frac{\partial A}{\partial\theta}\right) + \lambda_0^2 A = 0. \quad (11)$$

The solution to our boundary value problem for the dipolar case is

$$A_{\text{lin}} = B_0 r_0^2 \sin^2\theta \frac{a_0 J_{3/2}(\lambda_0 r) + b_0 J_{-3/2}(\lambda_0 r)}{a_0 J_{3/2}(\lambda_0 r_0) + b_0 J_{-3/2}(\lambda_0 r_0)}\sqrt{\frac{r}{r_0}}. \quad (12)$$

Provided that λ_0 is not a root of

$$a_0 J_{3/2}(\lambda_0 r_0) + b_0 J_{-3/2}(\lambda_0 r_0) = 0, \quad (13)$$

the free constants a_0 and b_0 generate multiple solutions to our boundary-value problems for each given λ_0. If λ_0 is a root of equation (13), the boundary value problem has no solution. These are well-known results in the Sturm-Liouville theory (Courant & Hilbert 1963a). However, the above solutions are physically not interesting because the total magnetic energy,

$$E = \int_{r > r_0} \frac{B^2}{8\pi}\, dV, \quad (14)$$

in each case is unbounded owing to a characteristically slow decline of $|\boldsymbol{B}|$ to zero at $r \to \infty$ (Berger 1985; Low 1996). On

the other hand, the limit $\lambda_0 = 0$ gives the potential field A_{pot} with a finite total energy E, as can be verified. In other words, the potential field is a singular limit of $\lambda_0 \to 0$.

Since lines of force are lines along which A takes a constant value, the roots r of

$$a_0 J_{3/2}(\lambda_0 r) + b_0 J_{-3/2}(\lambda_0 r) = 0 \qquad (15)$$

for a given λ_0 define an infinite set of concentric spheres that are flux surfaces. The linear force-free fields are each an infinite set of closed magnetic fluxes separated by these concentric spheres, a property relevant to § 2.2. It is clear that force-free magnetic fields in the unbounded domain $r > r_0$ of finite total energy generally requires Q to be a nonlinear function of A.

2.2. *The Total Magnetic Energy*

The virial theorem of Chandrasekhar (1961) shows that the total magnetic energy of a force-free magnetic field in a domain V is uniquely given by the vector values of the field at the boundary ∂V

$$\int_V \frac{B^2}{8\pi} \, dV = \int_{\partial V} \frac{B^2}{8\pi} (\mathbf{r} \cdot d\mathbf{S}) - \int_{\partial V} \frac{1}{4\pi} (\mathbf{B} \cdot \mathbf{r})(\mathbf{B} \cdot d\mathbf{S}), \quad (16)$$

where $\mathbf{r}$ is the position vector in spherical coordinates and $d\mathbf{S}$ is the surface area element directed out of V. In axisymmetry, the energy of a force-free magnetic field in an interior domain $r < r_0$ of a rigid boundary $r = r_0$ is given by

$$E = \frac{1}{4} r_0^3 \int_0^\pi \left(B_\theta^2 + B_\varphi^2 - B_r^2 \right)_{r=r_0} \sin \theta \, d\theta. \qquad (17)$$

For a fixed boundary flux B_r at $r = r_0$, the more highly twisted the force-free field is, the greater are the boundary values of the tangential components B_θ and B_φ at $r = r_0$. In particular, solutions exist for $B_r = 0$ on $r = r_0$ for a magnetic field entirely contained in $r < r_0$. Examples of such fields are easy to construct with linear force-free magnetic fields corresponding to $b_0 = 0$ in equation (12), imposed to ensure regularity of the field at the origin.

The force-free fields in the exterior $r > r_0$ of the rigid boundary $r = r_0$ is distinctly different, as revealed by its energy integral

$$E = \frac{1}{4} r_0^3 \int_0^\pi \left(B_r^2 - B_\theta^2 - B_\varphi^2 \right)_{r=r_0} \sin \theta \, d\theta, \qquad (18)$$

where it is assumed that $\mathbf{B}$ declines to 0 at infinity sufficiently rapidly to ensure that the total magnetic energy is finite. Here we see that for a fixed normal field B_r at $r = r_0$, one cannot assume that a highly twisted field attributed with large prescribed values of B_φ at $r = r_0$ is allowed. For example, it is not to be taken for granted that any prescribed $Q(A)$ in equation (7) can give a physical solution in $r > r_0$ satisfying boundary conditions (8).

Whereas in the case of the domain $r < r_0$ a force-free field may exist with $B_r = 0$ on $r = r_0$, no force-free field can exist in $r > r_0$ with $B_r = 0$ on $r = r_0$ (Low 2001). In the former, the tangential magnetic field along the boundary $r = r_0$ exerts a pressure force that is taken up by that rigid boundary to confine the field within the finite volume. In the latter, the absence of an outer boundary above $r = r_0$ means that any

field not threading across $r = r_0$ will expand to fill all space and approach a state of diluted field indistinguishable from vacuum. Only fields threading across $r = r_0$ may exist in a force-free state, with the part of the field anchored to $r = r_0$ serving to transmit the self-confining magnetic tension force on to the inner boundary.

The requirement of $B_r \neq 0$ on $r = r_0$ is only a necessary condition for a force-free field to exist in $r > r_0$. By virtue of the energy being positive, equation (18) sets an upper bound on the form of $Q(A)$ defining the force-free field in terms of the given boundary flux,

$$\int_0^\pi \left(B_r^2 - B_\varphi^2 \right)_{r=r_0} \sin \theta \, d\theta > 0, \qquad (19)$$

which translates into the condition on $Q(A)$ for the boundary value problem based on conditions (8) and (9)

$$\int_0^\pi \left[q(A)^2 \right]_{r=r_0} \frac{d\theta}{\sin \theta} < \frac{8}{3}, \qquad (20)$$

where we have written $Q = B_0 r_0 q(A)$ to put a bound on q as a dimensionless quantity.

2.3. *Power-Law Force-Free Magnetic Fields*

The preceding analysis suggests that it would be interesting to investigate the family of force-free fields generated for $Q(A)$ as a fixed function of A with a free constant amplitude to be increased monotonically from zero until the limit for existence of solutions is approached. The limit set by inequality (20) is not the lowest upper limit. With no loss of generality, let us use physical units such that $r_0 = 1$ and $B_0 = 1$. This paper is centered on the study of

$$[Q(A)]^2 = \frac{2\gamma}{n+1} A^{n+1}, \qquad (21)$$

introducing the constant n and the constant amplitude γ. The governing equation is then

$$\frac{\partial^2 A}{\partial r^2} + \frac{\sin \theta}{r^2} \frac{\partial}{\partial \theta} \left(\frac{1}{\sin \theta} \frac{\partial A}{\partial \theta} \right) + \gamma A^n = 0. \qquad (22)$$

For a given n, we wish to generate the solutions in $r > 1$ subject to the boundary conditions (8) and (9) as the value of γ is increased monotonically from 0. Nonlinear elliptic partial differential equations present formidable questions of existence and uniqueness of solutions (e.g., Courant & Hilbert 1963b; Lazer & McKenna 1980; Esteban 1991). The power-law for $Q(A)$ is mathematically the simplest form to adopt. In many physical applications, the flux function A decays to zero in the far reaches of the domain. The power law provides an instructive case of how Q might decay as a monomial in A across the flux surfaces of constant A with its implications for the field's self-confinement. We take a numerical approach to equation (22) in our study.

Constant values of the magnetic stream function A define magnetic flux surfaces. Equation (21) thus prescribes a loading of B_ϕ, which exerts a magnetic pressure across these flux surfaces, declining with a power law in A. We study the implication of the rate of decline on global equilibrium, taking n to be even integers, which ensures that the right hand side of equation (21) is positive definite independent of the sign of A.

When $\gamma = 0$, we have the potential dipole field given by the flux function (10). For γ small, we expect a solution in small departure from the potential field in the domain. Taking the far field in $r > 1$ to be the potential dipole field in the leading term, it can be shown that the nonlinear source term in equation (22) evaluated with that leading term does not produce a meaningful first order correction if $n \leq 3$. This suggests that solutions in the neighborhood of the potential dipole field, subject to boundary conditions (8), require $n > 3$ (Low 1986). Therefore, we chose the cases of $n = 5$, 7, and 9 for treatment. Inequality (20) sets the following upper bound on γ above which no solution to the boundary value problem can exist

$$\gamma < \frac{2(n+1)(2n+1)!!}{3(2n)!!} \qquad (23)$$

for each value of n, where $(2n + 1)!! = (2n + 1)(2n - 1)\ldots(3)(1)$ and $(2n)!! = (2n)(2n - 2)\ldots(4)(2)$.

2.4. *The Aly Magnetic Energy*

It useful for our purpose to introduce the Aly magnetic energy (Aly 1984, 1991; see also Sturrock 1991; Wolfson 1993). The axisymmetric magnetic fields in $r > 1$ may be classified into the class of fields each with all lines of force anchored at the two ends on the boundary $r = 1$, and the complement class of fields containing an azimuthal rope of flux located entirely in $r > 1$ running around the axis of symmetry. This flux rope has lines of force projected into closed curves of constant A located entirely in $r > 1$ in the r-θ plane. We call the former fully anchored fields, or just anchored fields for short, and the latter flux-rope fields.

Two energy bounds are interesting. The first is that any force-free magnetic field satisfying boundary conditions (8) and (9) has an energy in excess of E_{pot} of the potential magnetic field given by equation (10). The second bound is due to Aly energy. Consider all magnetic fields, not necessarily in equilibrium, with one end of each line of force anchored to $r = 1$ and the other out to infinity, satisfying boundary conditions (8) and (9). Among these fields, the one with the lowest energy is potential everywhere except for a current sheet in the equator, where the bipolar field reverses sign abruptly. Denote the total energy of this minimum-energy state by E_{Aly}. For the dipolar field $E_{Aly} = 1.66E_{\text{pot}}$ (Low & Smith 1993). We accept Aly's conjecture that for any fully closed, anchored force-free field satisfying boundary conditions (8) and (9), its total energy E_{fff} satisfies the inequality

$$E_{\text{pot}} < E_{fff} < E_{\text{Aly}}. \qquad (24)$$

This inequality implies that none of the closed anchored force-free magnetic fields with the same boundary flux at $r = 1$ may have enough stored magnetic energy to drive an outflow that opens up every line of force to infinity.

Inequality (24) does not apply to flux-rope fields (Aly 1991). It is therefore interesting to seek examples in which the Aly limit on anchored fields might be exceeded by flux-rope fields. Recently, Wolfson (2003) produced a numerical example of a flux-rope force-free field demonstrating such an energy excess of the order of only a few percent, an excess not to be accepted conclusively, as the author had cautioned, in view of the numerical uncertainty of the method of solution employed. Hu, Li, & Xing (2003) also reported a possible excess of energy, of less than 10%, of a low-β flux-rope equilibrium field over the Aly energy produced by a time-dependent relaxation

to a static state. The excess over the Aly energy may not be large because the first term in the integrand of equation (18) is an absolute upper bound on the energy. Denoting this absolute upper bound by E_{abs}, we have for all force-free fields, both anchored and with flux ropes,

$$E_{\text{abs}} = \frac{1}{4}\int_0^\pi \left(B_r^2\right)_{r=1} \sin\theta\, d\theta > E_{fff}. \qquad (25)$$

For the dipolar boundary conditions (8) and (9), $E_{\text{abs}} = 2E_{\text{pot}}$. Moreover, E_{abs} is not the least upper bound. Hence, an excess above the Aly limit in a flux-rope magnetic field is moderate, $E_{\text{abs}} = 2E_{\text{pot}} > E_{fff} > E_{\text{Aly}} = 1.66E_{\text{pot}}$, with E_{fff} expected to be closer to E_{Aly} than E_{abs}, since a purely radial field at the boundary, in order to attain the high value of E_{abs}, is not likely to be force-free.

2.5. *Self-similar Fields*

The power-law force-free fields were studied by Low & Lou (1990). They found separable solutions of the form

$$A = \frac{H_m(\theta)}{r^k}, \qquad (26)$$

where $k + 2 = kn$ and H_m is the solution to a nonlinear eigenvalue problem for each fixed n, associated with the integer m to label the parameter γ as an eigenvalue. These solutions are self-similar by virtue of its invariance to a scaling of the radial coordinate. These self-similar solutions have been studied in the context of astrophysical accretion disks, including the fitting of these self-similar solutions to parametrically varied boundary conditions at the accretion disks (Uzdensky 2002; Lynden-Bell & Boily 1994; Wolfson 1995).

Now the self-similar force-free fields are solutions to boundary conditions (8) for the flux, with $r_0 = 1$ for $F(\theta)$ given by

$$F = H_m(\theta). \qquad (27)$$

In the theory of Barenblatt & Zel'dovich (1972), self-similar solutions may be of greater general interest than might have been implied by their rather particular forms. The self-similar solutions are associated with the absence of an intrinsic scale so that the solutions are each invariant to a scale transformation. Then, in the idea of the intermediate asymptotics of Barenblatt & Zel'dovich, self-similar solutions may be the leading order approximation of solutions to a boundary value problem in a locality of the domain far from the boundary of the domain. In such a locality, scales deriving from the far boundary conditions become mathematically irrelevant. For example, such scales may be lodged not in the leading-order term but in the higher order terms of the local expansion. As we set out in the next section to generate families of nonlinear force-free fields, we watch out for the existence of such intermediate asymptotic localities where the self-similar force-free fields of Low & Lou may be found.

3. THE NUMERICAL BOUNDARY VALUE PROBLEM

There are several challenges associated with the numerical solution of the boundary value problem posed by equations (22), (8), and (9)

Infinite domain.—This needs to be truncated to a finite computational domain with an appropriate radiation boundary condition to simulate its infinite extent and incorporate the far-field asymptotic knowledge.
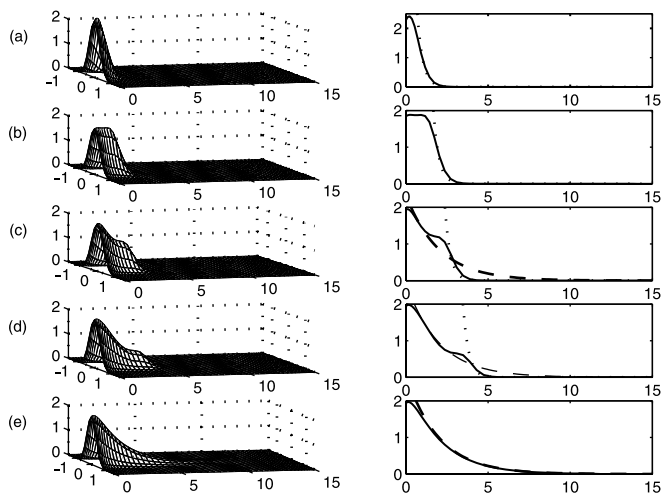
Fig. 1.—Samples of solutions along the continuous solution branch to eq. (22) for $n = 5$. *Left column*: $A(s, \eta)$ in the computational s-η plane at the marked locations in Fig. 2 with $s\epsilon[0, 15]$ and $\eta\epsilon[-\pi/2, \pi/2]$. *Right column*: corresponding radial decay rate of the field along $\eta = 0$ ($\theta = \pi/2$). The dotted line is a decay rate of $\exp(-3s)$, characteristic of the potential dipole decay rate [note: $\exp(2s)\exp(-s)^5 = \exp(-3s)$]. The dashed line is a decay rate of $\exp(-\frac{1}{2}s)$, characteristic of a self-similar solution with a dipolar topology [note: $\exp(2s)\exp(-\frac{1}{2}s)^5 = \exp(-\frac{1}{2}s)$].

Nonlinear equations.—The iteration method to be used must converge rapidly, independent of whether or not the underlying physical problem is time-stable. Newton's method is a natural choice (Fornberg 1988).

High-order accuracy is needed for derivative approximations.—The cost of Newton's method, our method of choice, increases very rapidly with the number of grid points, which therefore needs to be kept as low as possible.

Solution branches must be followed past turning points in γ.—For each value of the parameter γ, multiple solutions or possibly infinitely many solutions may exist, requiring special care in linking the different branches of solutions.

The numerical procedure, coded in MATLAB, used in this work was designed to resolve these difficulties. We describe this procedure in the Appendix, with a discussion of its important mathematical features: (1) Transforming the truncated computational domain $(1 < r < r_\infty, \; 0 < \theta < \pi/2)$, for some sufficiently large r_∞, into the logarithmically stretched rectangular domain $s = \log r$, $\eta = \pi/2 - \theta$. This will transform equation (22) into

$$\frac{\partial^2 A}{\partial s^2} - \frac{\partial A}{\partial s} - \frac{\partial^2 A}{\partial \eta^2} + \tan\eta \frac{\partial A}{\partial \eta} + \gamma e^{2s} A^n = 0.$$

(2) Use of Chebyshev-spaced grid points in the s-direction. (3) Approximation of derivatives by pseudospectral methods (Fornberg 1996); (4) use of either the Dirichlet or radiative boundary conditions at the outer boundary; and, (5) use of pseudo-arc length continuation for following solution branches through their turning points (Keller 1987; Allgower & Georg 1992).

Here we present the solutions we have obtained for the contrasting cases of $n = 5$, 7, and 9.

3.1. *The $n = 5$ Sequence*

Figure 1 shows the general character of the sequence of solutions to the boundary value problem for $n = 5$. With use

of the pseudo-arc length continuation scheme described in the Appendix, it becomes irrelevant from a numerical perspective that the solution sequence features turning points in γ. A straightforward implementation of the Newton's iteration method with γ as a free parameter would fail in the vicinity of the turning points. Therefore, we do not describe the behaviors of the solution A in terms of γ values, but in terms of positions on the solution curve. We have displayed five samples from the continuous solution curve.

The first column displays representative solutions in the sequence in terms of the nonlinear term $\gamma \exp(2s)A^5$ in the transformed computational domain (s, η). The second column displays the corresponding solutions as a function of s along the line $\eta = 0$, which corresponds to the equatorial plane $\theta = \pi/2$ of the unit sphere. Figure 2 displays the total magnetic energy (in units of potential energy) and flux along the continuous solution curve with the marked points (a)–(e) corresponding to the solutions (a)–(e) displayed in Figure 1. The graph of the total magnetic energy versus γ clearly shows that solutions are found by our numerical methods only for $\gamma \leq 2.32$, a more stringent bound on γ than that set by inequality (23) for $n = 5$,

$$\gamma < 10.82, \tag{28}$$

for the existence of a solution. The bound in inequality (28) is not the least upper bound on γ for the existence of a solution. On the other hand, we cannot rule out the possibility that other solutions, not found by our numerical procedure, may exist such that $2.32 < \gamma < 10.82$.

A physical interest of our mathematical study is to discover a local maximum in A in the domain for some value of γ. Such a maximum would represent a magnetic flux rope with its field line projections on the physical r-θ plane in the form of closed curves of constant A (Chen 1989; Low 1996; Zhang & Low 2003, 2004). No maximum of A was found in our $n = 5$ sequence of solutions. The solution given in row 1 in Figure 1 suggests a hint of a maximum forming in $\gamma \exp(2s)A^5$. Careful examination of the neighborhood of this solution in terms of A showed that no maximum actually formed. At most an
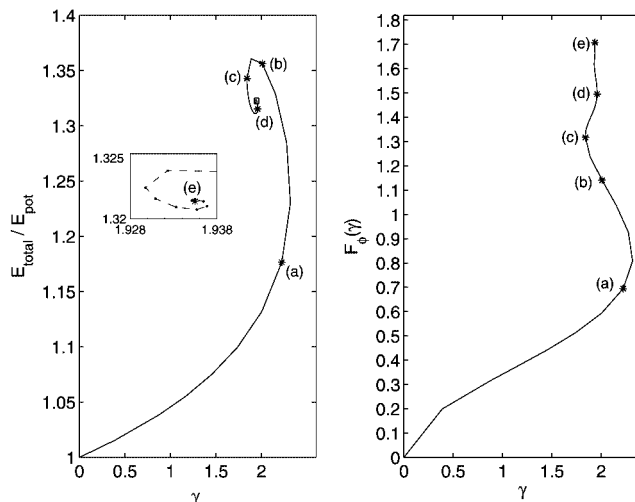
Fig. 2.—Energy (in units of potential energy) and magnetic flux vs. γ along the solution curve for $n = 5$. The five samples in Fig. 1 are correspondingly labeled at points (a)–(e).

inflection point might have formed and then disappeared as we move along the solution curve.

The solutions do display an interesting property in its decay to zero in the far reaches of the atmosphere. In the second column of Figure 1, the graph of $\gamma \exp(2s)A^5$ along the equator $\theta = \pi/2$ is plotted against two different decay rates, one at the rate of $\exp(-3s)$ (*dotted line*), characteristic of the potential dipole field, and the more gradually decaying $\exp\left(-\frac{1}{2}s\right)$ (*dashed line*), characteristic of a self-similar solution with a dipolar topology. As we go down the column from the top we see solutions with a dipolar potential decay evolve parametrically to those with the self-similar decay. The solution curve in Figure 2 curls into a limiting point not resolved at the level of numerical resolution we employed. The evolution in the decay rate of the solution is discernible upon crossing the turning point at $\gamma = 2.32$ and the self-similar decay takes over completely in the far region as the limiting solution is reached at $\gamma = 1.93$. Our solution sequence shows that, as we proceed along the solution curve, the far field solution becomes less sensitive to the form of the Dirichlet boundary condition at $r = 1$ and assumes a self-similar form as its lead approximation, in the manner described by Barenblatt & Zel'dovich (1972).

The computational domain we employed is radially sufficiently extended so that the outer boundary conditions, whether based on the potential dipole decay rate or the self-similar decay rate, produced the same solution because the two exponential decay rates are sufficiently severe to have their values at this outer boundary falling below machine accuracy.

3.2. *The Total Azimuthal Magnetic Flux*

To provide a physically more intuitive interpretation of the $n = 5$ solution curve, we calculate the total magnetic flux in the φ-direction in the atmosphere

$$F_\varphi = \int_{r>1} B_\varphi r \, dr \, d\theta, \qquad (29)$$

along the solution curve, displayed in Figure 2 alongside the graph for the total magnetic energy. The spiraling part of the graph for the total energy shows that the limiting point is approached with an oscillation of the total energy above and below that of the limiting point. In contrast, the total azimuthal flux F_φ is monotonically increasing along the solution curve.

Physically, we are looking at a sequence of force-free fields characterized with a monotonically increasing total azimuthal flux F_φ. The solution curve may be parameterized mathematically more conveniently by F_φ instead of γ. The former is one-to-one whereas the latter involves different branches with the same value of γ associated with more than one solution on the curve. Note that, despite the monotonic increase of F_φ along the solution curve, the magnetic energy is not a monotonic function of F_φ, a point we have more to say in the conclusion of the paper.

In each force-free field, its azimuthal flux is held in equilibrium by the part of its dipolar poloidal field anchored to $r = 1$. The amount of anchored dipolar flux is independent of F_φ, fixed by boundary conditions (8) and (9). The azimuthal field B_φ produces two forces, a magnetic pressure force and a magnetic tension force, the latter directed at the axis of symmetry. These forces are to be balanced by the magnetic pressure and tension forces contributed by the poloidal field generated by A. The force balance equation written in the form

of equation (5) has conveniently reduced the effect of B_φ to just the force due to an isotropic formal pressure $Q^2/2$ in the r-θ plane. The increase of F_φ is effected with the profile of $Q(A)$ kept in an invariant form—the assumed power law in A. The increase in F_φ is complicated by the dependence of A on space changing from one solution to another. Thus, F_φ is a global or integral function of $Q(A)$, and not a simple linear function of γ. Consequently, the physics in terms of F_φ is easier to interpret than in terms of γ.

With a monotonically larger total azimuthal flux to be confined by a fixed amount of anchored poloidal flux, along the solution curve, the field progressively expands radially outward to relieve the magnetic pressure $Q^2/2$. In so doing, the poloidal flux is also stretched radially outward. Equilibrium in this situation then depends critically on whether the reduced strength in the stretched poloidal field is sufficient to confine the reduced magnetic pressure of the stretched azimuthal flux. The self-similar solution of Low & Lou for a fixed index n may be characterized by its property that the radial decay of B_φ as represented by Q is precisely the same as the decay of the poloidal field as represented by A/r, as functions of r. The identical decay is the basic reason that both poloidal and azimuthal fields are scale-invariant. The evolution of the decay in Figure 1 along the solution curve may be understood in terms of how the increasingly large azimuthal flux F_φ is confined with this scale-independent distribution expanding to ever larger extent radially outward. The limiting point indicates in Figure 2 that there is a maximum value of about 1.7, in the units used, for F_φ to be accommodated in this particular mechanical mode. Exceeding this maximum value must require a change in the nature of confinement or a loss of confinement.

The former may correspond to a smooth continuation into a new sequence of equilibria such as one with a different functional form of $Q(A)$. The loss of confinement is more interesting. It could be produced by a dynamical transition in which a part of the poloidal flux, upon failing to confine the excessive azimuthal flux, is pushed open to allow the azimuthal flux to propagate out as nonlinear shear Alfvén waves (Low 1986; Wolfson & Low 1992; Aly 1995; Uzdensky et al. 2002). With
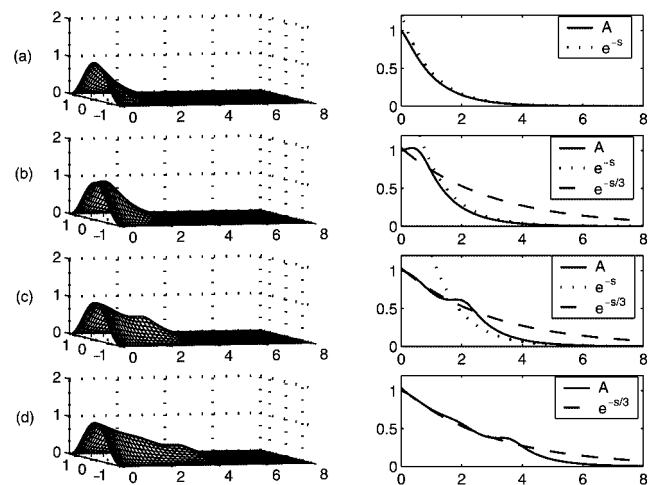
FIG. 3.—Samples of solutions along the continuous solution branch to eq. (22) for $n = 7$. *Left column*: $A(s, \eta)$ in the computational s-η plane at the marked locations in Fig. 5 with $s\epsilon[0, 8]$ and $\eta\epsilon[-\pi/2, \pi/2]$. *Right column*: corresponding radial decay rate of the field along $\eta = 0(\theta = \pi/2)$.
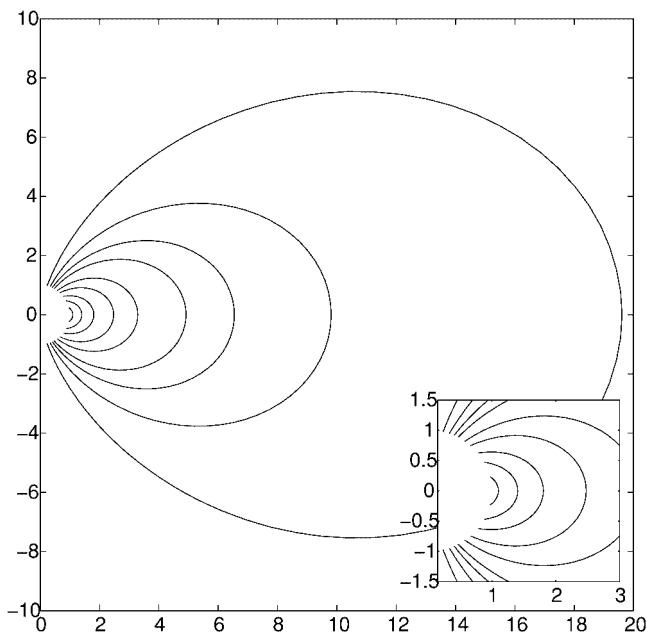
Fig. 4a
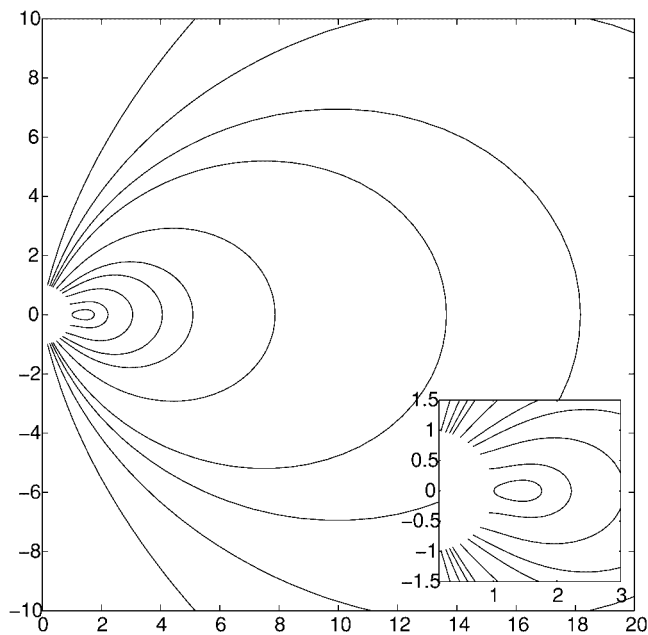
Fig. 4b
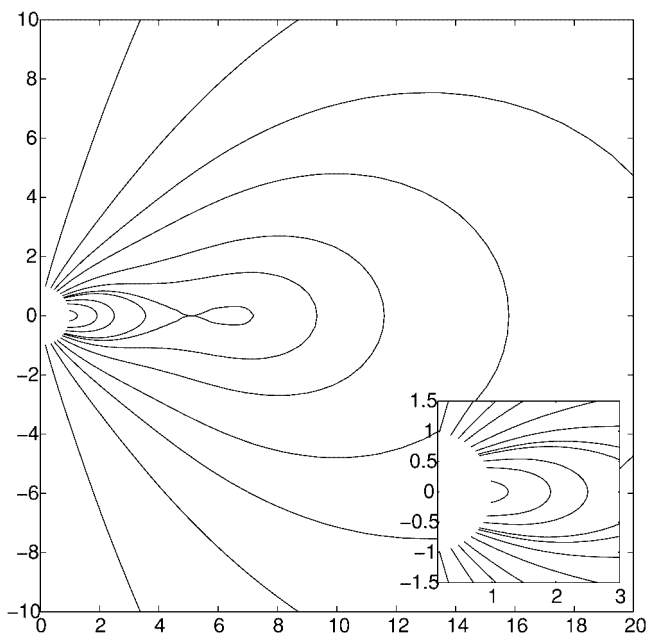
Fig. 4c
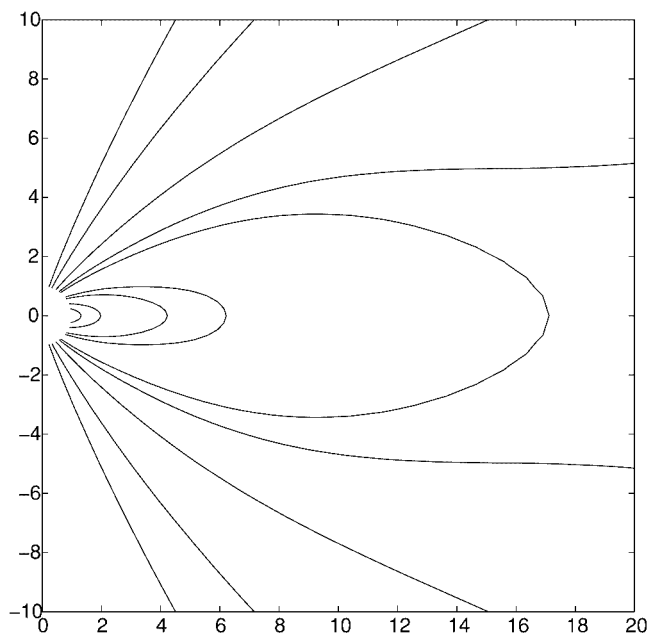
Fig. 4d

Fig. 4.—Corresponding contour plots of the A field in the physical r-θ plane for $n = 7$ at the marked location in Fig. 5

a loss of azimuthal flux via such an opening-up process, the anchored poloidal flux will eventually dominate again to re-close by magnetic reconnection, producing a new equilibrium with a reduced F_φ. In this transition, the end state is likely to be an equilibrium with $Q(A)$ taking some form determined by the details of the dynamical transition. The $n = 5$ sequence in Figures 1 and 2 suggests a general conclusion that with a fixed poloidal flux anchored to $r = 1$, only a limited amount of azimuthal flux may be confined by it. There may be a maximum azimuthal flux associated with a given profile of A on $r = 1$, independent of the form of $Q(A)$. We can not be sure that the maximum is 1.7 as obtained by the power-law case of

$n = 5$, but we suggest that this value characterizes its order of magnitude for the dipolar case given by equations (8) and (9).

3.3. *The $n = 7$ Sequence*

The $n = 7$ sequence is presented in Figures 3, 4, and 5, in a format that shows directly the formation of a magnetic flux rope in the atmosphere. On the left column of Figure 3 are the two-dimensional plots of the flux function $A(s, \eta)$ at different points on the continuous solution curve. A local maximum in A is clearly discernible in the second and third plots from the top. The runs of A along the equator $\theta = \pi/2$, displayed as a function of s along $\eta = 0$, show the formation of the maximum
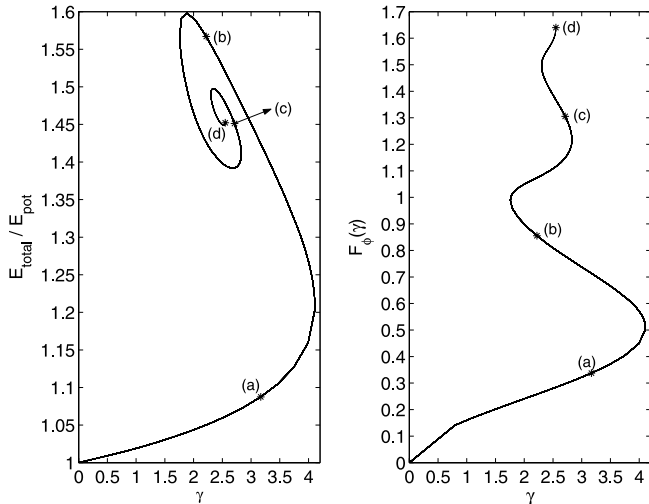
Fig. 5.—Energy (in units of potential energy) and magnetic flux vs. γ along the solution curve for $n = 7$. The four samples in Figs. 3 and 4 are correspondingly labeled at points (a)–(d).

more clearly. The dotted curves and the broken curves are the decay profiles for the dipolar potential flux function $[\exp(-s)]$ and the $n = 7$ self-similar decay $[\exp(-s/3)]$. We see that solution A starts along the solution curve with a potential decay rate and spreads its azimuthal flux radially outward and evolving toward a self-similar profile as we progress along the solution curve.

Figure 4 displays the four flux functions shown in the left column of Figure 3, as lines of force of the magnetic field in the physical r-θ plane. The sequence shows first the formation of a flux rope of closed A-lines near the base $r = 1$, which progresses out into the atmosphere. This rope reduces in size parametrically as it separates from the bipolar field underneath the rope by an X-type magnetic neutral point. Eventually the rope disappears and the field relaxes toward the $n = 7$ self-similar profile for the far field everywhere, as the solution terminates in the limiting point of the energy curve in Figure 5.

In contrast to the $n = 5$ sequence, the energy curve for the $n = 7$ sequence has a more pronounced spiral to the limit point. As in the case of the $n = 5$ sequence, the $n = 7$ sequence has a monotonically increasing total azimuthal flux F_φ along the solution curve. Note that the maximum value of F_φ is again of the order of 1.7, despite the difference in the power indices of $Q(A)$ as a power-law dependence on A. In both cases, the azimuthal flux F_φ is confined by the same amount of poloidal flux defined by boundary conditions (8) and (9). This result lends support to our suggestion that the given poloidal flux anchored to $r = 1$ is capable of confining a total azimuthal flux of that maximum magnitude.

The maximum value of γ for which solutions exist is about 4 in the case of $n = 7$, larger than the case of $n = 5$. This means that the former may have solutions with a larger maximum value in the azimuthal field component B_φ, located at a maximum value of A than the case of $n = 5$. The $n = 7$ flux rope is tightly wound and confined near $r = 1$. This local property is controlled by the index n, although the maximum total amount of azimuthal flux to be confined by the fixed amount of poloidal flux appears not to be sensitive to the index n.

The Aly energy $E_{\rm Aly}$ becomes an interesting quantity to consider since it is not, in principle, a bound of the total energy of a force-free field with a flux rope. The total magnetic energies, given in units of potential energy, for the four

examples in the left column in Figure 3 and Figures $4a$–$4d$ are 1.09, 1.57, 1.45, and 1.45, respectively. Figure 5 shows that the maximum total energy attained in the sequence is a flux-rope solution with a total energy of 1.598. For the boundary flux fixed by boundary conditions (8) and (9), $E_{\rm Aly} = 1.66$ in the same units. Thus, the maximum energy of 1.598 of the sequence is about 4% short of the Aly energy. Since all units are given in potential energy $E_{\rm pot} = 1$, implying a threshold of $E_{\rm Aly} - E_{\rm pot} = .66$ as the energy required to stretch all the anchored poloidal field to open up to infinity. The maximum energy of the sequence has exceeded $E_{\rm pot}$ by the amount 0.598 of the order of 90% of the threshold. The trend suggested by the $n = 5$ and 7 sequences points to the possibility that $n = 9$ might have a maximum energy that does exceed the Aly energy.

3.4. *The $n = 9$ Sequence*

Figures 6, 7, and 8 display the $n = 9$ sequence of force-free fields, in the same format of representation as Figures 3–5 for the $n = 7$ sequence. As expected, a maximum in A, representing a flux rope, emerges in the sequence of states associated with a monotonically increasing azimuthal total magnetic flux; see the example in rows (b) and (c) in Figure 6 and the corresponding plots of the poloidal lines of force in the r-θ plane shown in Figure 7. Of particular note is the large magnetic flux rope located above an X-type magnetic neutral point in Figure 7c. The spiraling solution curve in the energy versus γ plot is not only more tightly wound than the lower n cases, it also intersects itself at multiple points. At each such intersection, the two magnetic fields are not the same, but they share the same total energy and value of γ. The tightly wound spiral curve represents a parametric oscillation of the total energy in the solution curve characterized by a monotonically increasing total azimuthal flux, shown on the right in Figure 8.

The limit point in Figure 8 correspond to a field that has a $n = 9$ self-similar form extending out to infinity. This state is the state of maximum total azimuthal flux in the sequence. This maximum value is once again about 1.7 in the dimensionless unit used, an additional piece of numerical evidence that the fixed amount of poloidal flux, anchored to $r = 1$, may confine only a maximum amount of azimuthal flux of that order of magnitude.
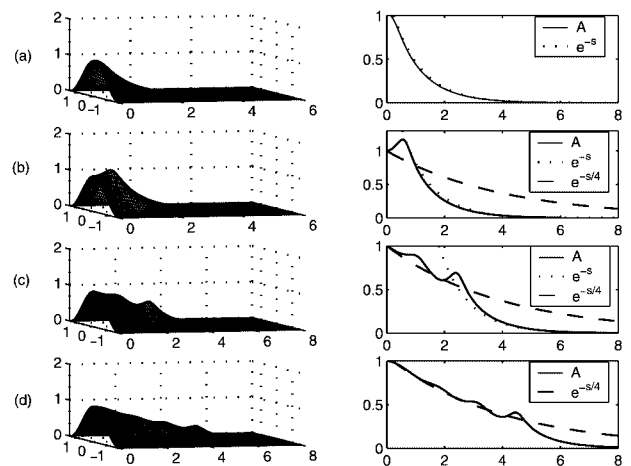
Fig. 6.—Samples of solutions along the continuous solution branch to eq. (22) for $n = 9$. *Left column*: $A(s, \eta)$ in the computational s-η plane at the marked locations in Fig. 8 with $s\epsilon[0, 6]$ and $\eta\epsilon[-\pi/2, \pi/2]$. *Right column*: corresponding radial decay rate of the field along $\eta = 0$ ($\theta = \pi/2$).
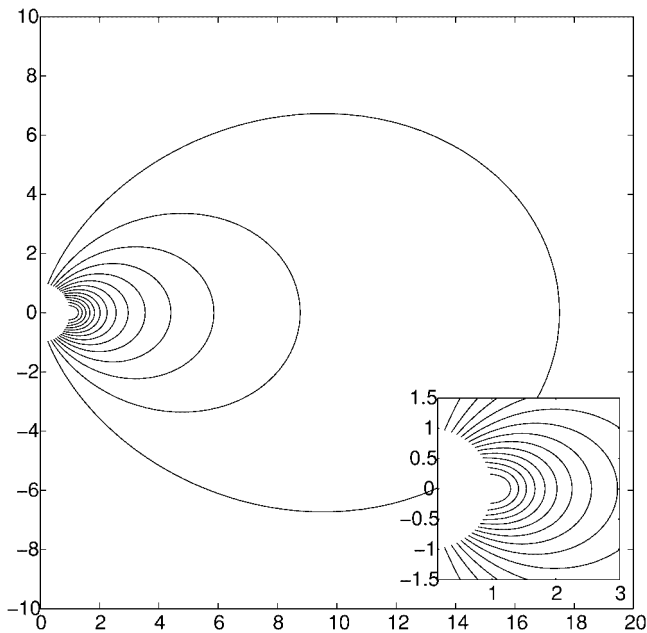
Fig. 7a
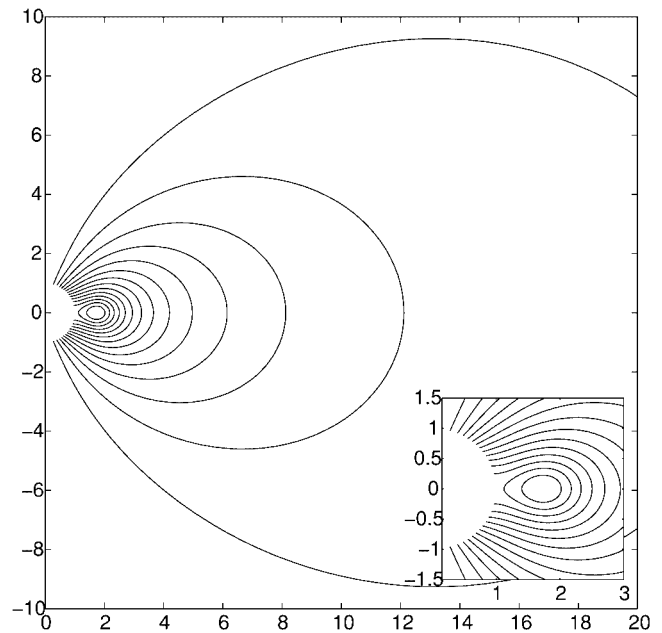
Fig. 7b
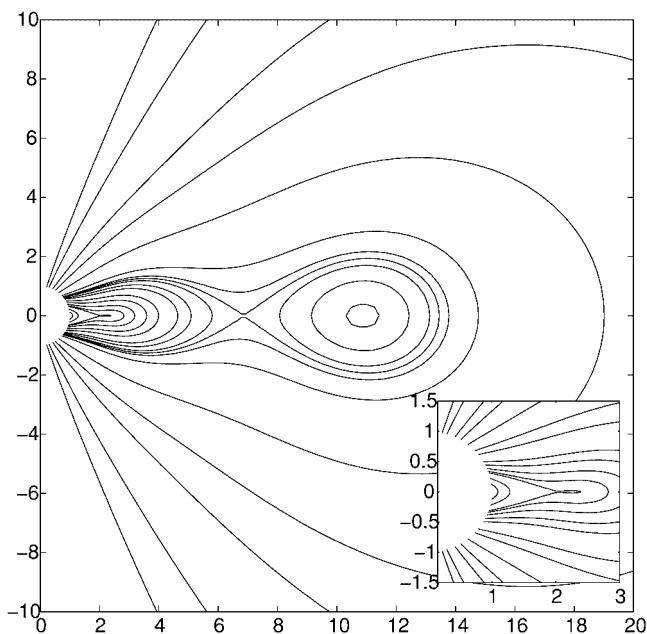
Fig. 7c
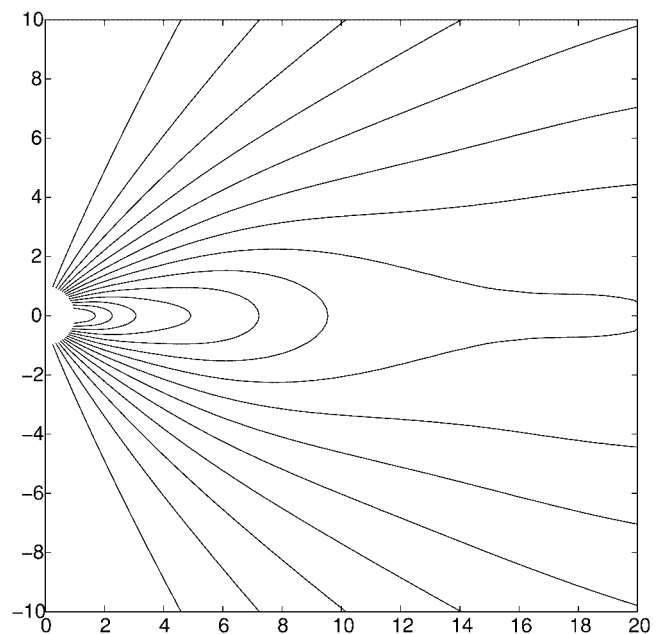
Fig. 7d

Fig. 7.—Corresponding contour plots of the A field in the physical r-θ plane for $n = 9$ at the marked location in Fig. 8

More interesting is the largest total magnetic energy realized along the solution curve. Figure 8 shows that this maximum is a little below 1.73 but has exceeded the Aly energy by about 3.5% of the Aly energy. Figure 9 shows the monotonically increasing trend in the respective maximum magnetic energies of the sequences $n = 5$, 7, and 9, displayed against the energy levels corresponding to E_{pot}, E_{Aly}, and E_{abs}. The maximum total energy of the $n = 9$ sequence is obtained in the neighborhood of the state displayed in Figure 7b. Note in the insert figure of this state that the flux rope is confined low in atmosphere, with a deformation of the neighboring lines of force outside the flux rope toward normal incidence at $r = 1$. Examination of the virial formula for the total energy,

equation (18) shows that the total energy is rendered large for those fields with small root mean squared B_θ and B_φ on $r = 1$, with B_r at $r = 1$ fixed by the boundary conditions of the problem. These two conditions are met in the state in Figure 7b. Near normal incidence of the poloidal field at $r = 1$, as shown, gives a small rms B_θ at $r = 1$. The relatively high value of $n = 9$ implies a steep decline of Q as we leave the maximum of A by virtue of the power-law dependence of Q or, more physically, B_φ. This implies that the rms B_φ at $r = 1$ is also minimal.

The steepness of the gradients of Q as a power-law function of A in the case $n = 9$ requires extremely high spatial resolutions for their numerical computation. The redeeming factor,
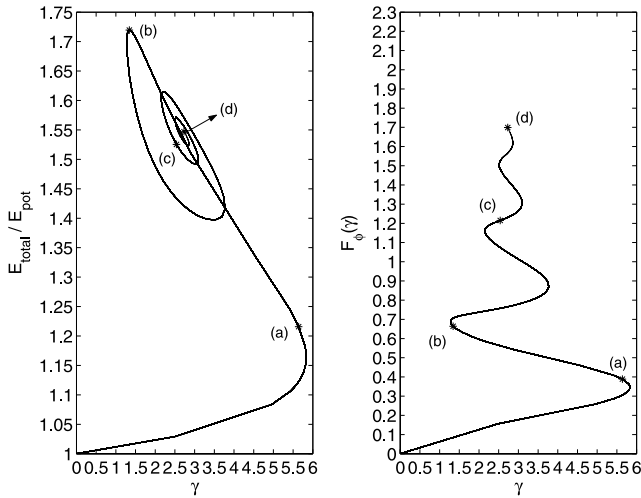
FIG. 8.—Energy (in units of potential energy) and magnetic flux vs. γ along the solution curve for $n = 9$. The four samples in Figs. 6 and 7 are correspondingly labeled at points (a)–(d).

however, is that as the power-law index increases, the decay rate of the nonlinear term in equation (A1) goes as $\exp[(-n + 2)s]$. The computation was done on two separate grids to verify that the maximum energy had exceeded the Aly energy by 3.5% with numerical confidence. Since there is little change in the azimuthal direction between cases, the grid needed to be refined in the radial direction. The first grid was a coarser grid of 127 points (radial) and 31 points (azimuthal) on a domain from 0 to 8 and $-\pi/2$ to $\pi/2$. Taking advantage of the exponentially rapid decline of A with s, we reduce the radial size of the domain from $[0, \, 8]$ to $[0, \, 6]$, achieving a grid refinement in the radial direction with 81 points (radial) and 31 points (azimuthal) on a domain from 0 to 6 and $-\pi/2$ to $\pi/2$. In the first case the maximum energy exceeded the Aly limit by 3.4% and in the second case by 3.6%. The insensitivity of the calculation to the grid size gives numerical confidence in the estimate.

4. SUMMARY AND CONCLUSION

The solar expulsion of a large-scale magnetic structure known as a CME motivates this mathematical study of nonlinear force-free magnetic fields in the unbounded domain representing an open atmosphere. Nonlinear boundary value problems are notoriously intractable, in general, and little is known about force-free fields in the unbounded domain with their confinement properties. The different sequences of power-law, axisymmetric, force-free fields constructed with the numerical solver described in the Appendix provide explicit solutions to illustrate these confinement properties.

These axisymmetric fields attain equilibrium by confining a given amount of azimuthal flux within a poloidal field anchored at both ends of the lines of force to the inner boundary $r = 1$. Each sequence is characterized by a fixed amount of the confining poloidal flux but an increasing amount of azimuthal flux. The intensity of the poloidal field is controlled by its spatial expansion to fill the unbounded domain under the divergence-free condition (2) and subject to a fixed amount of that flux being anchored to the inner boundary. This dictates how much poloidal flux may expand outward to confine a given amount of azimuthal flux without becoming so weak as to fail confinement.

The power-law index n controls how rapidly the azimuthal field $B_\varphi = Q(A)/r \sin \theta$ varies across the poloidal flux surfaces of constant A. With A declining to zero in the far region, the greater n is, the more rapidly Q declines across the flux surfaces to the far region. In the outer far region the poloidal field, constrained by the requirement of a global equilibrium, may decay radially more rapidly than the azimuthal field does. When this happens, confinement must fail. We have not directly demonstrated the failure of confinement. Such a demonstration is mathematically difficult and outside the scope of the present paper. What we have demonstrated with these sequences of solutions is that the self-similar solutions of Low & Lou (1990) appear to be a preferred means by which a power-law force-free field achieve the equilibrium between the poloidal and azimuthal fields. This scale-invariant balance of force spreads parametrically to fill all space as a means for the field to accommodate an increasing amount of total azimuthal flux. It is interesting that this total azimuthal flux may not be increased unbounded, with the maximum allowable attained when the self-similar force-balance has extended all the way out to infinity.

For large enough n, the localization of Q as a power of A allows for the equilibrium to embed an azimuthal rope of twisted flux. This occurs in the neighborhood of $n \geq 7$ if the amplitude of Q is within a certain range. It is interesting that taking $n = 9$ allows for such a flux rope field to have a total energy in excess of the Aly energy. This excess is moderate, on the order of a few percent of the Aly energy in the $n = 9$ case. This result corroborates similar results by Hu et al. (2003) and Wolfson (2003), treating distinctly different models.

Two important physical implications should be mentioned in relation to the CME phenomenon. Our solutions make the following basic point about magnetic fields in the force-free state in an unbounded space. Such a field counts on the anchoring of a certain amount of flux at the inner boundary to hold the field in equilibrium. Detached fields have a general tendency to expand. Confinement is possible whenever the anchoring effect of the field dominates. This naturally suggests that if the amount of anchored flux is fixed, the amount of unanchored flux must not exceed a certain threshold if it is to be trapped in a force-free state in the anchored flux. The termination of our solution curves at about the same amount of maximum total azimuthal flux, not sensitive to n, suggests that
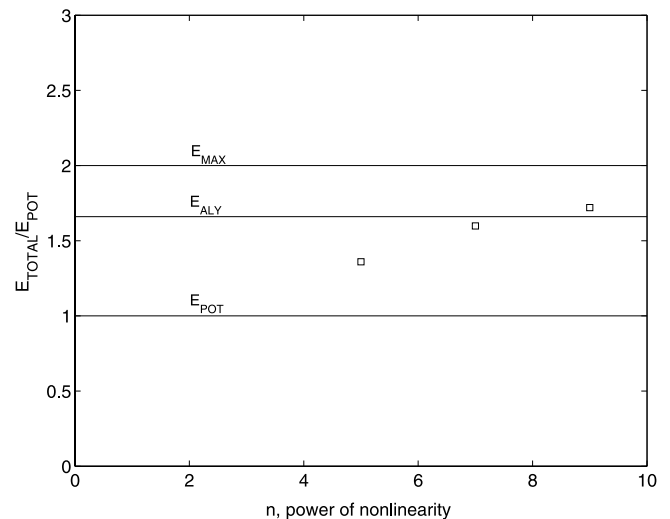
FIG. 9.—Energy vs. power-law index, n

this is a plausible physical result. This result may not even be sensitive to the form of $Q(A)$, but its order of magnitude may be fixed largely by the poloidal flux anchored and distributed in a particular way at $r = 1$ in our axisymmetric model. Proving this result is an interesting problem in mathematical hydromagnetics.

In realistic three-dimensional geometry, there is no need for a detached flux, that is, a flux completely detached from the boundary, to result in a loss of self-confinement. A given amount of flux anchored to the inner surface may be highly twisted without a detached flux rope. If the twist is too large, such as measured by the total relative helicity of such a field (Berger & Field 1984; Zhang & Low 2003), the field may fail confinement by its inability to keep the twist within the field in equilibrium. Then, the field would expand outward driven by the nonlinear Alfven waves carrying the twist to the far reaches of the atmosphere (Roussev et al. 2003).

The second implication is that to fully open an axisymmetric field by the field's stored energy, there is little excess in the stored energy over the Aly energy. The greater the azimuthal flux given to the poloidal field of a fixed amount, the greater the stored energy. But, there is a limit to how much azimuthal flux one could put into the field within the capability of magnetic self-confinement. This limit is problematical for the explanation of the energetics of CMEs requiring more energy for each CME than can be found in the Aly energy (Low & Smith 1993). The matter is radically different if there are additional nonmagnetic forces available to allow an even greater stressing of the field (Zhang & Low 2004). In other words, if there is a nonmagnetic agent to confine the magnetic field, then a greater amount of energy may be stored. Observations suggest that the weight of plasmas trapped in the field in the form of prominences and coronal helmet structures may provide this additional means of field confinement (Low 2001; Fong, Low, & Fan 2002; Low, Fong, & Fan 2003; Zhang 2003). This possibility will be examined in the follow-up paper.

APPENDIX A

THE DESIGN OF THE NUMERICAL SOLVER

As a first step toward addressing the four challenges given in § 3, equation (22) is rewritten in the form

$$\frac{\partial^2 A}{\partial s^2} - \frac{\partial A}{\partial s} + \frac{\partial^2 A}{\partial \eta^2} + \tan \eta \frac{\partial A}{\partial \eta} + \gamma e^{2s} A^{1+2/p} = 0, \tag{A1}$$

under the coordinate transformation $s = \ln r$, $\eta = \pi/2 - \theta$. The sequence $p = 1, \frac{1}{2}, \frac{1}{3}, \frac{1}{4}, \ldots$ corresponds to $n = 1 + 2/p = 3, 5, 7, 9, \ldots$. The transformed computational domain $-\pi/2 \le \eta \le \pi/2, 0 \le s \le \infty$ is then truncated at $s = s_\infty$, a constant, which is equivalent to e^s solar radii. Thus, the outer boundary can be placed sufficiently far to serve as an approximation to the unbounded domain of the original problem. The domain is then discretized on a $M \times N$ grid, with M equispaced points in the η-direction and N Chebyshev-spaced points in the s-direction, i.e., $s_k = \{1 - \cos[\pi(k-1)/(N-1)]\}s_\infty/2, \ k = 1, 2, \ldots, N$. All derivatives were then approximated by standard pseudospectral (PS) methods (Fornberg 1996), utilizing the periodicity in the η-direction. These approximations are most conveniently viewed as global finite difference formulas, with weights provided, e.g., by the algorithms given in Weideman & Reddy (2000). At all boundaries (apart from $s = s_\infty$, which will be discussed below), the boundary conditions can be implemented immediately. Considering the A-values at all the grid points as unknowns, we have thus obtained MN equations for MN unknowns. This nonlinear system of equations is then solved by Newton's method (see e.g., Fornberg 1988 for a discussion of a similar implementation in the case of a steady flow problem).

We describe next the code in three parts: (1) code for the case in which the parameter γ is fixed, and the outer boundary condition is $A = 0$ at $s = s_\infty$, (2) radiation boundary conditions at $s = s_\infty$, and (3) pseudo–arc length continuation for following solution branches through their turning points.

A1. PARAMETER γ FIXED; OUTER BOUNDARY CONDITION $A = 0$ AT $s = s_\infty$

The unknown A-values are defined on an $M \times N$ grid. We reorder them by columns, from left to right, into a single vector of length MN. We then order the governing equations associated with each grid point correspondingly. This nonlinear system has a Jacobian matrix, structured as shown in Figure 10. In the $N \times N$ block structure (shown in case of $N = 10$), the blocks are of size $M \times M$. The matrix entries are the partial derivatives of the different equations with respect to the unknowns (A-values), evaluated based on the current approximate solution.

The right-hand side contains the negative of the residual when the current approximate solution is substituted into the governing equations, and the solution vector then gives the updates to the unknowns. With γ fixed, Newton's method converges quadratically whenever the initial guess for the solution is sufficiently close to a (nonmultiple) solution. Until we approach a turning point (at which γ changes direction when we follow the solution branch), the very crude initialization $A \equiv 0$ turns out to suffice. However, using the solution from a previous γ-case is usually more effective.

If we had used second-order finite differences (FD2; instead of PS) to approximate the space derivatives, the matrix shown in Figure 10 would instead be block-tridiagonal, with the central blocks internally tridiagonal, and the remaining ones diagonal. The change from FD2 to PS in the η-direction only fills in entries within that band structure, and does therefore not noticeably affect the computational cost. For the same accuracy, a far lower value of M can be used. Since the cost with respect to changes in M scales as
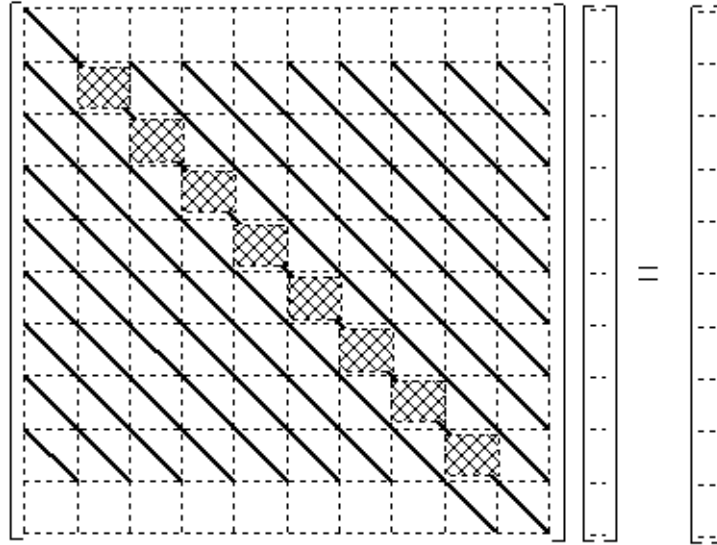
Fig. 10.—Block Structure of the linear system to be solved using Newton's method in the case of γ fixed and a Dirichlet far field boundary condition. The central (hatched) blocks are full matrices and the others are each diagonal matrices indicated by a diagonal line. Zero matrices are represented by empty blocks along the top and bottom rows.

$O(M^3)$, the benefits in using PS in the η-direction are critical in permitting solutions with the needed accuracy. In the s-direction, the situation is a bit more complex, since going from FD2 to PS changes the matrix structure from banded to full. With respect to N, the solution costs in the two cases are $O(N)$ versus $O(N^3)$, respectively. The truncation errors are $O(1/N^2)$ versus $O(e^{-cN})$ (for some constant $c > 0$). Hence, to reach an accuracy level of ε, the costs incurred will scale like $O(1/\sqrt{\varepsilon})$ and $O\left(\ln\frac{1}{\varepsilon}\right)^3$, respectively. When $\varepsilon \to 0$, the PS approach is therefore again the clear winner. We implemented both the FD2 and PS approaches, and actual timings confirmed that the costs for the FD2 approach was prohibitive on standard workstations.

A2. RADIATION BOUNDARY CONDITION AT $s = s_\infty$

Although we are not solving a problem with physical radiation, the phrase ''radiation boundary condition'' is here used to denote a boundary condition that incorporates far-field asymptotic information in a nontrivial way, in order to permit a relatively small computational domain (a situation that is often encountered when solving problems involving physical radiation). We encounter two different kinds of far field behaviors for solutions to (A1). Their analytic character and the appropriate far-field radiation conditions for them are discussed next.

A2.1. *Dipole Far Field*

We drop the nonlinear term in equation (A1) and look for separated solutions of the form $A(s, \eta) = S(s)H(\eta)$. This leads to

$$\frac{1}{S}\left(\frac{d^2S}{ds^2} - \frac{dS}{ds}\right) + \frac{1}{H}\left(\frac{d^2H}{d\eta^2} + \tan\eta\frac{dH}{d\eta}\right) = 0, \tag{A2}$$

requiring that $H(\eta)$ satisfies $H_{\eta\eta} + \tan\eta\, H_\eta = -\lambda H$. Together with the boundary conditions $H(\pm\pi/2) = 0$, this equation has the eigenvalues $\lambda_k = k(k+1)$, $k = 1, 2, 3, \ldots$, and corresponding eigenfunctions $H_1(\eta) = -\cos^2\eta$, $H_2(\eta) = -\sin\eta\cos^2\eta$, etc. In the s-direction, the decay rates become e^{-ks}, $k = 1, 2, 3, \ldots$ Since we are only interested in solutions that are symmetric around $\eta = 0$, we need only consider k odd. For s large, the first mode therefore strongly dominates the far field. This is numerically implemented by letting the bottom right block in the Jacobian contain I (the identity matrix) and the block to the left of it $-\exp[-(s_n - s_{n-1})]I$.

A2.2. *Similarity Solution Far Field*

Without dropping the nonlinear term, we can still find a particular separated solution to (A1) $A(s, \eta) = e^{-ps}H(\eta)$, where $H(\eta)$ will now satisfy

$$\frac{d^2H}{d\eta^2} + \tan\eta\frac{dH}{d\eta} + p(p+1)H + \gamma H^{1+2/p} = 0, \tag{A3}$$

recalling $p = 1, \frac{1}{2}, \frac{1}{3}, \frac{1}{4}, \ldots$ This equation, with the same boundary conditions $H(\pm\pi/2) = 0$ as before, can be viewed as a nonlinear eigenvalue problem. For any values of γ and p, it has infinitely many solutions $H(\eta)$. Their decay rates are given by e^{-ps},

and the radiation boundary condition can therefore be implemented by letting the matrix block to the left of the bottom right block instead be $- \exp[-p(s_n - s_{n-1})]I$.

A3. PSEUDO-ARC LENGTH CONTINUATION

With the procedure described above, we can compute the A-fields for a sequence of γ-values, as long as the sequence is monotonically increasing or decreasing. However, at turning points, the Jacobian matrix becomes singular, and continuing in γ fails. Instead of using γ as an independent variable and computing $A(\gamma)$, we introduce a function of A, such as the energy $E(A)$, and consider the curve $E(A)$ versus γ. Along this curve, we can introduce the arc length σ as a new independent variable. Working with $A(\sigma)$ and $\gamma(\sigma)$ converts turning points to regular points. The modifications this requires in the Newton scheme have been described numerous times in the literature, (e.g., Keller 1987; Allgower & Georg 1992), and they lead to what are known as arc length (or pseudo−arc length) continuations. Treating γ also as a dependent variable means that the structure of the Jacobian matrix in Figure 10 gets altered by the inclusion of an additional column. The difficulty lies in where to find an additional governing equation (since attempting to directly specifying an increment in σ leads to a singular Jacobian). In the procedure that we implemented, the (now rectangular) Jacobian matrix is first decomposed as RQ, where R is upper triangular and Q is orthogonal. It can then be shown that adding a row $[0, 0, \ldots, 0, 1]$ to the bottom of the R-matrix achieves the goal. Very heuristically, this works because it corresponds to advancing the solution according to the last row of the orthogonal matrix Q, i.e., in the only direction that the governing equations do not specify. This therefore has to be in the direction along the arc. Since a QR (or RQ) decomposition has twice the operation count of Gaussian elimination, the computational cost becomes twice as large as in the case in which γ is given. The complete code amounts to about 60 lines of MATLAB and runs in a matter of seconds (or up to a few minutes) per iteration on a standard PC for the grid sizes that were used in the present work. Thanks to the Newton method's quadratic convergence, four iterations are typically needed to obtain convergence to machine precision for our discrete nonlinear systems (note, however, that the discrete solutions differ from the continuous ones because of truncation errors. These errors are typically much larger and depend on the numerical step sizes in the two spatial directions and on how close the outer boundary is placed).

REFERENCES

Allgower, E. L., & Georg, K. 1992, Acta Num., 1, 64
Aly, J. J. 1984, ApJ, 283, 349
———. 1991, ApJ, 375, L61
———. 1995, ApJ, 439, L63
Antiochos, S. K., DeVore, C. R., & Klimchuk, J. A. 1999, ApJ, 510, 485
Barenblatt, G. I., & Zel'dovich, Ya. B. 1972, Annu. Rev. Fluid Mech., 4, 285
Berger, M. A. 1985, ApJS, 59, 433
Berger, M. A., & Field, G.B. 1984, J. Fluid Mech., 147, 133
Chandrasekhar, S. 1961, Hydrodynamic and Hydromagnetic Stability (Oxford: Oxford Univ. Press)
Chen, J. 1989, ApJ, 344, 1051
Ciaravella, A., et al. 2000, ApJ, 529, 575
Courant, R., & Hilbert, D. 1963a, Methods of Mathematical Physics, Vol. 1 (Amsterdam: Academic Press)
———. 1963b, Methods of Mathematical Physics, Vol. 2 (Amsterdam: Academic Press)
Dere, K. P., Brueckner, G. E., Howard, R. A., Michels, D. J., & Delaboudiniere, J. P. 1999, ApJ, 516, 465
Esteban, M. J. 1991, Commun. Pure Appl. Math., 44, 259
Fong, B., Low, B.C., & Fan, Y. 2002, ApJ, 571, 987
Fornberg, B. 1988, J. Fluid Mech., 190, 471
———. 1996, A Practical Guide to Pseudospectral Methods (Cambridge: Cambridge Univ. Press)
Gibson, S. E., & Low, B. C. 1998, ApJ, 493, 460
———. 2000, J. Geophys. Res., 105, 18187
Howard, R. A., Sheeley Jr., N. R., Koomen, M.J., & Michels, D. J. 1985, J. Geophys. Res., 90, 8173
Howard, R. A., et al. 1997, Geophys. Monogr., 99, 17
Hu, Y. Q., Li, G. Q., & Xing, X. Y. 2003, J. Geophys. Res., 108, 1072
Hundhausen, A. J. 1999, in The Many Faces of the Sun, ed. K. Strong, J. Saba, B. Haisch, & J. Schmelz (New York: Springer), 143

Keller, H. K. 1987, Lectures on Numerical Methods in Bifurcation Problems (New York: Springer)
Klimchuk, J. A., & Sturrock, P. A. 1989, ApJ, 345, 1034
Lazer, A. C., & McKenna, P.J. 1980, in Differential Equations, ed. S. Ahmad, M. Keener, & A. C. Lazer (Amsterdam: Academic Press), 199
Low, B. C. 1977, ApJ, 212, 234
———. 1978, ApJ, 224, 668
———. 1986, ApJ, 307, 205
———. 1990, ARA&A, 28, 491
———. 1996, Sol. Phys., 167, 217
———. 2001, J. Geophys. Res., 106, 25141
Low, B. C., Fong, B., & Fan, Y. 2003, ApJ, 594, 1060
Low, B. C., & Lou, Y. Q. 1990, ApJ, 352, 343
Low, B. C., & Smith, D.C. 1993, ApJ, 410, 412
Lüst, R., & Schlüter, A. 1954, Z. Astrophys., 34, 263
Lynden-Bell, D., & Boiley, C. 1994, MNRAS, 267, 146
Parker, E. N. 1979, Cosmic Magnetic Fields (Oxford: Oxford Univ. Press)
Roussev, I., et al. 2003, ApJ, 588, L45
Sturrock, P. A. 1991, ApJ, 380, 655
Uzdensky, D. 2002, ApJ, 574, 1011
Uzdensky, D., Komigl, A., & Litwin, C. 2002, ApJ, 565, 1191
Weideman, J. A. C., & Reddy, S. C. 2000, ACM Trans. Math. Software, 26, 465
Wolfson, R. 1993, ApJ, 419, 382
———. 1995, ApJ, 443, 810
———. 2003, ApJ, 593, 1208
Wolfson, R., & Low, B. C. 1992, ApJ, 391, 353
Wolfson, R., & Saran, S. 1998, ApJ, 499, 496
Zhang, M. 2003, ApJ, submitted
Zhang, M., & Low, B. C. 2003, ApJ, 584, 479
———. 2004, ApJ, 600, 1043